Electronic Supplementary Information for

Molecular Mechanisms of Thermal Instability in Hybrid Perovskite Light Absorbers for Photovoltaic Solar Cells

Mingchao Wang[†*], Vallabh Vasudevan[†], Shangchao Lin[‡], Jacek Jasieniak[†], Salvy P. Russo[ǁ], Nick Birbilis[§] and Nikhil V. Medhekar[†*]

[†]Department of Materials Science and Engineering, Monash University, Faculty of Engineering, Wellington Road, Clayton, Victoria 3800, Australia

[‡]Institute of Engineering Thermophysics, School of Mechanical and Power Engineering, Shanghai Jiao Tong University, Shanghai 200240, China

[ǁ]ARC Centre of Excellence in Exciton Science, School of Science, RMIT University, Melbourne, Victoria 3001, Australia

[§]College of Engineering and Computer Science, Australian National University, Acton ACT 2601, Australia

*Corresponding Authors: mingchao.wang@monash.edu (Dr. Mingchao Wang);

nikhil.medhekar@monash.edu (A/Prof. Nikhil V. Medhekar).

S1. The analysis of radial distribution function and coordination numbers

In order to explore the microstructural evolution of bulk $MAPbI_3$ during melting process, we calculate radial distribution functions (RDFs) of Pb-I and I-I pairs for $MAPbI_3$ at different temperatures (T). For equilibrated $MAPbI_3$ at 300 K, **Figure S1(a)** shows two sharp RDF peaks of Pb-I pairs located at r = 3.08 and 7.0 Å, which represent I atoms in the octahedra connecting with center Pb atoms, and those in adjacent octahedra. With the increase of T, it can be seen in **Figure S1(b)** that both peaks become broadened meaning the large stretching of PbI_6 octahedra, but RDFs still maintain similar shapes up to T = 1052 K. We thus set the location of RDF valley right after the first RDF peak as Pb-I bond length cutoff, namely $r_{Pb\text{-}I}$ = 4.5 Å, which is then utilised for detecting Pb-I bonds in defective $MAPbI_3$. When gradually reaching melting point T_m ~1052 K, there is a sharp increase of first RDF peak, associated with the disappearance of the second RDF peak. Such variation in the trend for both RDF peaks demonstrates the crystalline-to-liquid phase transition, which is consistent with the calculation of translational order parameter η. Namely, the split of regular PbI_6 octahedra and formation of partial ones (i.e. PbI_4 and PbI_5) results in the enhanced first RDF peak of Pb-I pairs. Meanwhile, the lost medium-range order, as presented by the broken of PbI_6 octahedral network, leads to a significant reduction in the second RDF peak of Pb-I pairs. The RDFs of I-I pairs also show similar variation trend. As T increases, they have much broadened first peaks. This means wider range of I-I distances in PbI_6 octahedra, indicating much severer distortion of PbI_6 away from their regular shapes. When approaching T_m, the missing second and third RDFs peaks confirm again the existence of the short-range I-I order rather than the medium-range order.

S2 Phonon density of states and band structure calculations at finite temperature

To predict phonon density of states (DOS) and band structures at finite temperature, the dynamical matrix is first determined from MD simulations based on fluctuation-dissipation theory as implemented in LAMMPS. The simulation model has N = 10 × 10 × 10 unit cells ($MAPbI_3$ as one unit cell in this study), and each unit cell has three real space vectors, $\mathbf{a}_1$, $\mathbf{a}_2$ and $\mathbf{a}_3$. Based on the fluctuation-dissipation theory, the force constant coefficients are given by[1, 2]

$$\mathbf{\Phi}_{k\alpha,k'\beta}(\mathbf{q}) = k_B T \mathbf{G}^{-1}_{k\alpha,k'\beta}(\mathbf{q}) \tag{5}$$

where $\mathbf{q}$ is a reciprocal vector; $\mathbf{G}$ is the Green's functions coefficients given by

$$\mathbf{G}_{k\alpha,k'\beta}(\mathbf{q}) = \left\langle \mathbf{u}_{k\alpha}(\mathbf{q}) \cdot \mathbf{u}^{*}_{k'\beta}(\mathbf{q}) \right\rangle \tag{6}$$

where $\langle \cdots \rangle$ represents an ensemble average; $\mathbf{u}_{k\alpha}(\mathbf{q}) = \sum_l \mathbf{u}_{lk\alpha} \exp(i\mathbf{q} \cdot \mathbf{r}_l)$ is the α component of the atomic displacement for the kth atom in the unit cell in the reciprocal space at $\mathbf{q}$. In practice, $\mathbf{G}$ can also be measured based on the following expression

$$\mathbf{G}_{k\alpha,k'\beta}(\mathbf{q}) = \left\langle \mathbf{R}_{k\alpha}(\mathbf{q}) \cdot \mathbf{R}^{*}_{k'\beta}(\mathbf{q}) \right\rangle - \left\langle \mathbf{R}_{k\alpha}(\mathbf{q}) \right\rangle \cdot \left\langle \mathbf{R}^{*}_{k'\beta}(\mathbf{q}) \right\rangle \tag{7}$$

where $\mathbf{R}$ is the instantaneous positions of atoms, and $\langle \mathbf{R} \rangle$ is the averaged atomic positions. Once the force constant matrix is given, the dynamical matrix $\mathbf{D}$ can be obtained by

$$\mathbf{D}_{k\alpha,k'\beta}(\mathbf{q}) = (m_k m_{k'})^{-\frac{1}{2}} \mathbf{\Phi}_{k\alpha,k'\beta}(\mathbf{q}) \tag{8}$$

If the dynamical matrix $\mathbf{D}$ is known, its eigenvalues are exactly the phonon frequencies at $\mathbf{q}$. Therefore, you can predict the phonon band structures along certain reciprocal path. In addition, the phonon DOS can be obtained by integrating all $\mathbf{q}$ over the Brillouin zone.

For phonon dispersion calculation in this work, the 1 × 1 × 1 $MAPbI_3$ unit cell is expanded to 10 × 10 × 10 supercell to construct the perfect simulation model. Defective 1 × 1 × 1 $MAPbI_3$ unit cells with I and MA vacancies (vacancy concentration k_V = 2.5%) are expanded by 6 × 6 × 6 to construct corresponding defective simulation models.

Table S1. The detailed potential parameters for all intra-/inter-molecular interactions in hybrid perovskite $MAPbI_3$ from the potential MYP1.[3]

	Buckingham Potential		
Ion Pairs	**A (kcal/mol)**	**ρ (Å)**	**C (kcal/mol· Å^6)**
Pb – Pb	397000.0	0.28	25370.0
I – I	41319.0	0.46	10838.0
Pb – I	158565.0	0.32	11760.0
Pb – C	12566186.2765653	0.15	0.0
Pb – N	12566186.2765653	0.15	0.0
I – C	43412.8729434772	0.325	0.0
I – N	43412.8729434772	0.325	0.0
	Lennard-Jones Potential		
Ion Pairs	**ε (kcal/mol)**	**σ (Å)**	
C – C	0.1094	3.39967	
N – N	0.1700	3.25000	
HC – HC (-C)	0.0157	1.96000	
H+ – H+ (-N)	0.0157	1.06908	
Pb – HC (-C)	0.0140	2.70999	
Pb – H+ (-N)	0.0140	2.26454	
I – HC (-C)	0.0574	3.10000	
I – H+ (-N)	0.0574	2.75000	
Ion Type	**Partial charges q**		
Pb	+1.401200		
I	-0.700600		
N	-0.699800		
C	+0.460200		
HC (-C)	-0.003600		
H+ (-N)	+0.317000		

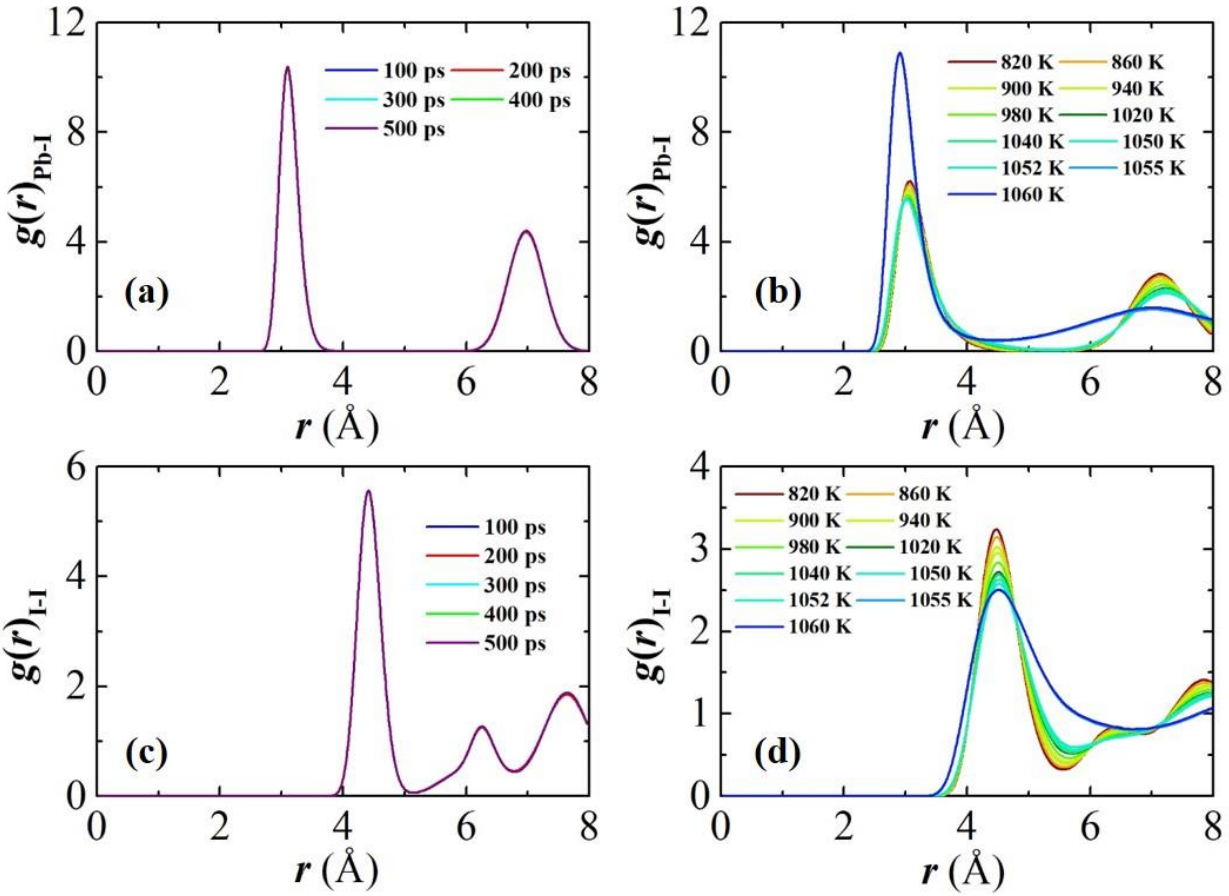

Figure S1. Radial distribution functions (RDFs) of atom pairs in pristine $MAPbI_3$ bulk crystal. (a-b) The RDFs of Pb-I pairs in $MAPbI_3$ (a) equilibrated at 300 K, and (b) heated up to the melting point $T_m \approx 1052.5$ K. (c-d) The RDFs of I-I pairs in $MAPbI_3$ (a) equilibrated at 300 K, and (b) heated up to the melting point $T_m \approx 1052.5$ K.

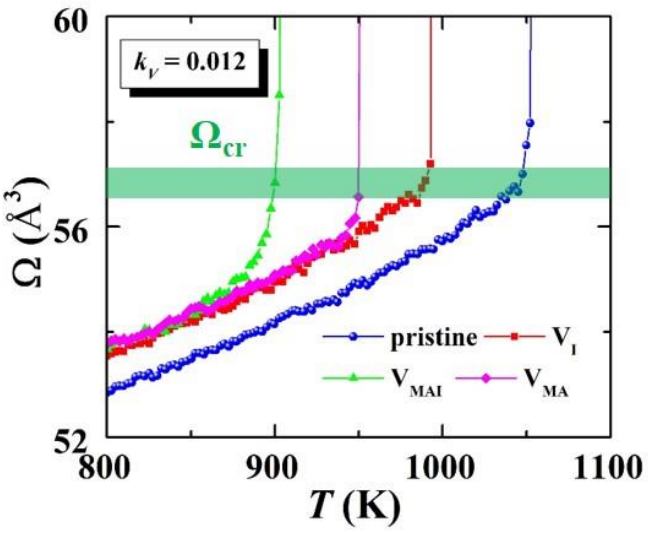

Figure S2. The mean atomic volume (Ω) of pristine and defective $MAPbI_3$ bulk crystals as a function of temperature (*T*). Three types of point defects, including I^- (V_I), MA^+ (V_{MA}), and MAI^0 (V_{MAI}) vacancies with a concentration of 0.012 are considered. The green bar highlights the critical mean atomic values Ω_{cr} when the melting of simulation models is initiated.

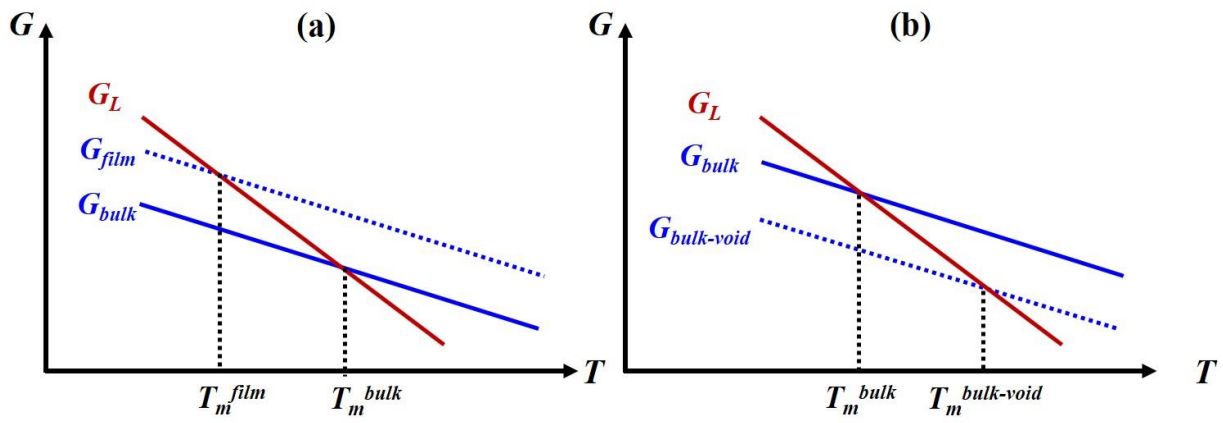

Figure S3. Schematic free energy diagram of the material melting of (a) thin films with free surfaces and (b) bulk crystals with nanovoids. See the main text for details. G_L, G_{bulk}, G_{film} and $G_{bulk\text{-}void}$ denotes the free energy of liquid phase, bulk crystals, thin films and bulk crystals with nanovoids. T_m^{bulk}, T_m^{film} and $T_m^{bulk\text{-}void}$ denote the melting temperatures of bulk crystals, thin films and bulk crystals with nanovoids.

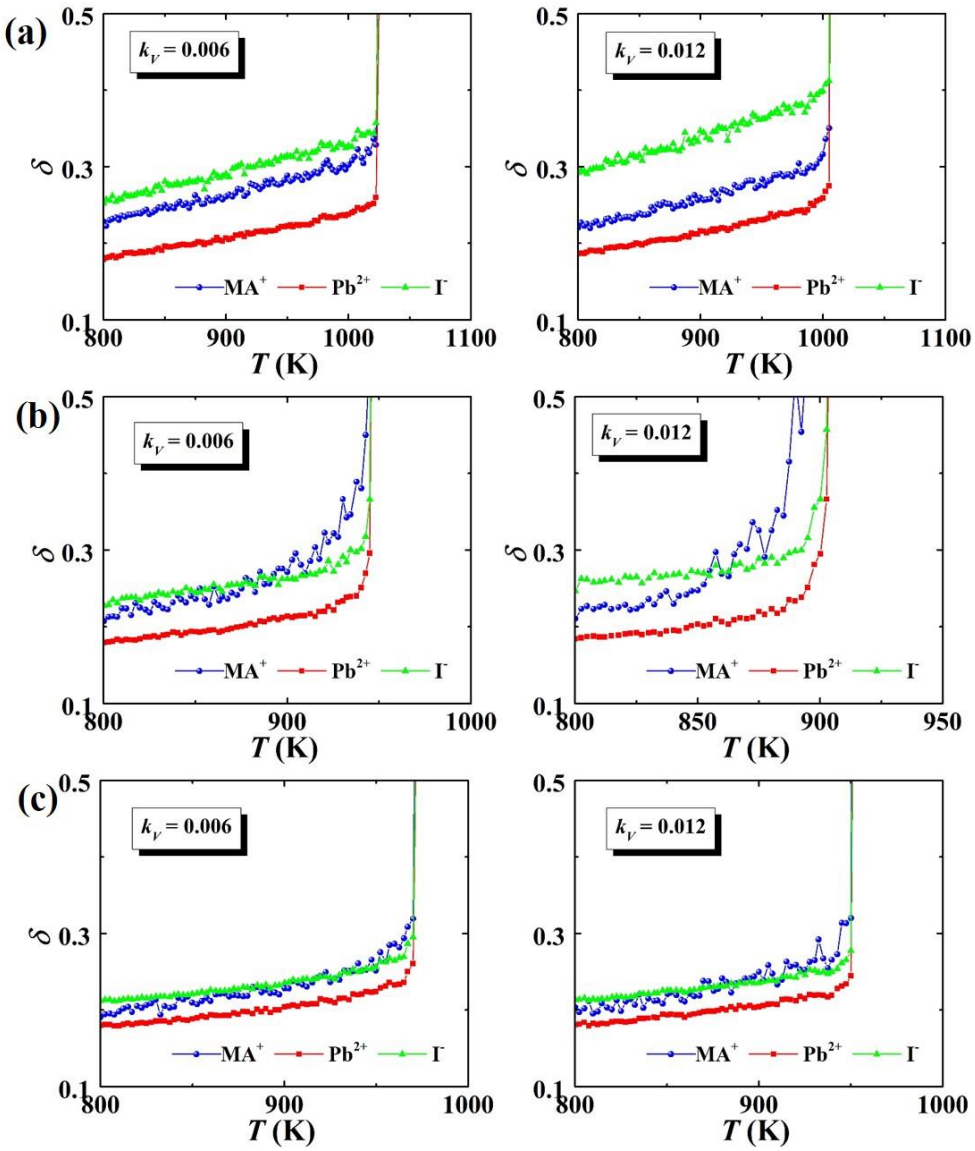

Figure S4. The Lindemann ratio of MA^+, Pb^{2+} and I^- ions in bulk $MAPbI_3$ with (a) I^-, (b) MAI^0 and (c) MA^+ vacancies at vacancy concentration k_V = 0.006 and k_V = 0.012 as a function of temperature *T*.

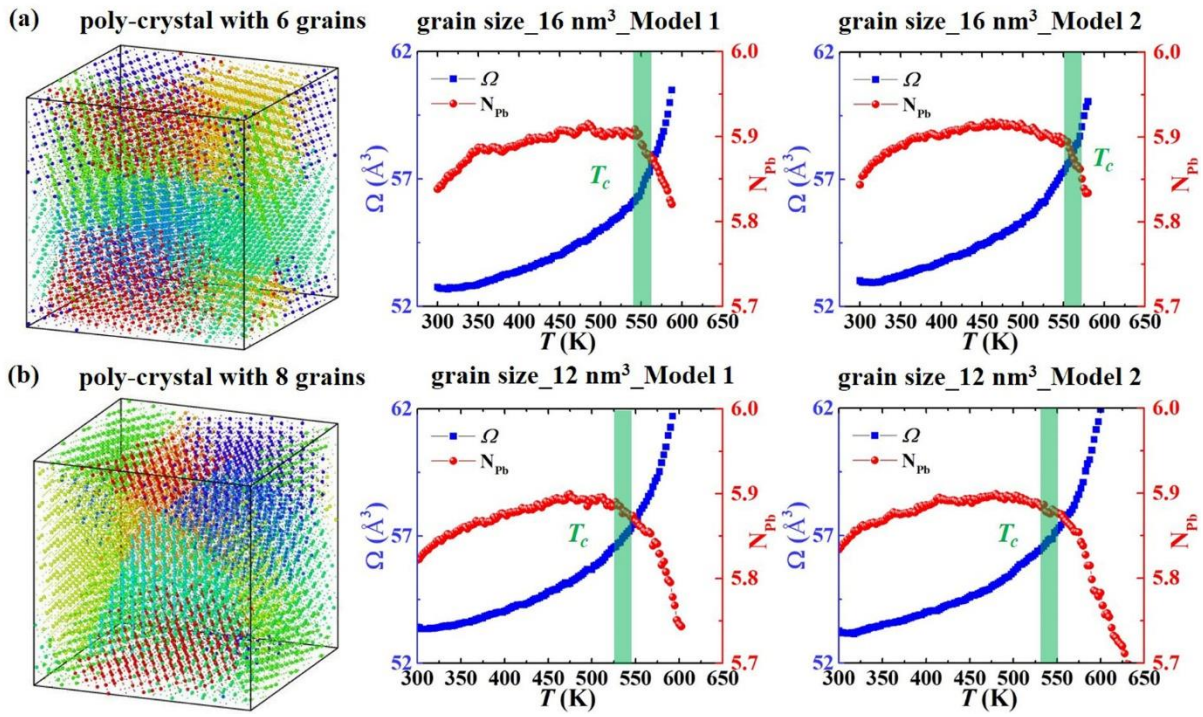

Figure S5. Atomistic configurations, as well as the mean atomic volume (Ω) and averaged coordination number of Pb ions (N_{Pb}) as a function of temperature for randomly oriented polycrystalline $MAPbI_3$ with the grain sizes of (a) 16 nm^3, and (b) 12 nm^3. Two different polycrystalline models with the same number of grains are simulated separately. The grain numbers of polycrystalline $MAPbI_3$ crystals are represented by different colors in the first column of figures.

References

(1) Campañá, C.; Müser, M. H. Practical Green's Function Approach to the Simulation of Elastic Semi-Infinite Solids. *Phys. Rev. B* **2006**, *74*, 075420.
(2) Kong, L. T.; Bartels, G.; Campañá, C.; Denniston, C.; Müser, M. H. Implementation of Green's function molecular dynamics: An extension to LAMMPS. *Comput. Phys. Commun.* **2009**, *180*, 1004-1010.
(3) Caddeo, C.; Saba, M. I.; Meloni, S.; Filippetti, A.; Mattoni, A. Collective Molecular Mechanisms in the $CH_3NH_3PbI_3$ Dissolution by Liquid Water. *ACS Nano* **2017**, *11*, 9183-9190.